Journal of Molecular Catalysis A: Chemical 325 (2010) 15–24

Contents lists available at ScienceDirect

Journal of Molecular Catalysis A: Chemical

journal homepage: www.elsevier.com/locate/molcata

A microkinetic model of ammonia decomposition on a Pt overlayer on Au(1 1 1)

Karsten Rasim[a,*], Manfred Bobeth[a], Wolfgang Pompe[a], Nicola Seriani[b,1]

[a] Institute for Materials Science and Max Bergmann Center of Biomaterials, Technische Universität Dresden, 01062 Dresden, Germany
[b] Fakultät für Physik, University of Vienna, Sensengasse 8, A-1090 Wien, Austria

ARTICLE INFO

Article history:
Received 6 October 2009
Received in revised form 15 March 2010
Accepted 16 March 2010
Available online 25 March 2010

Keywords:
Ammonia decomposition
Platinum
Gold
Kinetic model
Ab initio simulation

ABSTRACT

Ammonia decomposition is important for a series of technological applications. For developing efficient catalysts for this reaction, basic understanding of underlying mechanisms is fundamental. We have investigated ammonia decomposition on platinum (1 1 1) and (1 0 0) surfaces, and on a platinum overlayer on a (1 1 1) gold substrate within a microkinetic model. The kinetic parameters in the corresponding rate equations have been estimated on the basis of ab initio calculations of reaction and activation energies for the adsorption and dehydrogenation processes on the catalyst surface. Steady-state coverages of species participating in the decomposition have been determined as solution of the rate equations in the limiting case of small ammonia concentrations of an N_2–NH_3 model gas mixture under flow conditions. Calculated turnover frequencies of ammonia decomposition as a function of the temperature reproduce characteristic features reported for platinum wires. The highest turnover frequency and hydrogen coverage have been obtained for the platinum overlayer on gold. Potential application of this system as ammonia-sensing device is discussed.

1. Introduction

Ammonia is a compound of great technological importance. Its synthesis is sometimes considered as one of the most important technological developments of the 20th century [1]. Besides traditional applications as basic compound for producing various chemicals such as fertilizers [2,3], ammonia has recently gained attention also as hydrogen source for fuel cells [4,5] and as reducing agent for nitrogen oxides for automotive exhaust treatment [6]. In the latter applications, ammonia decomposition by heterogeneous catalysis plays a fundamental role. In fuel cells, catalysts are used to produce hydrogen by means of ammonia decomposition [7,8]. In exhaust treatment the remaining ammonia concentration after cleaning can be monitored by sensing changes of the hydrogen coverage on a catalytically active component. In the context of these technological applications, great efforts have been put in the development and characterization of particularly active catalysts for ammonia decomposition. Increasing interest in heterogeneous catalysis has recently been devoted to bimetallic systems as those systems are often more active than the pure components [9–13]. For example, few-monolayer-thick platinum films deposited on a gold substrate have been shown to have enhanced reactivity for oxidation reactions [9,14,15].

Motivated by these experimental investigations, we have theoretically studied ammonia decomposition on the platinum surfaces Pt(1 1 1), Pt(1 0 0), and on a Pt-monolayer (ML) on a Au(1 1 1) substrate, briefly referred to as Pt/Au(1 1 1) in the following. The kinetics of ammonia decomposition into hydrogen and nitrogen has been investigated within a microkinetic model describing ammonia adsorption and the consecutive dehydrogenation reactions on the catalyst surface. The kinetic parameters in this model have been estimated by calculating reaction and activation energies within the framework of density-functional theory (DFT). In the case of ammonia decomposition on Pt(1 1 1) and Pt(1 0 0), our results have been compared with the results of a thorough DFT analysis in a series of works by Offermans et al. and Novell-Leruth et al. [16–20]. In particular, frequency prefactors of rate constants in our microkinetic model have been chosen according to the DFT results of vibrational analysis in Ref. [19]. By means of our model, it is possible to predict the turnover frequency for ammonia decomposition which is usually measured in catalysis experiments. Concerning the potential application of the decomposition reaction for ammonia sensing, special focus in the present work is directed on the relationship between the ammonia pressure of the ambient gas and the hydrogen coverage on the different catalyst surfaces, with the aim to evaluate the suitability of Pt/Au(1 1 1) in comparison to pure platinum.

The paper is outlined as follows. In Section 2, computational details of our ab initio calculations are briefly described and the calculated adsorption and activation energies of surface reactions are

* Corresponding author. Current address: Institut des Materiaux Jean Rouxel (IMN), 2 rue de la Houssiniere, B.P. 32229, 44322 Nantes Cedex 3, France.
Tel.: +33 2 40 37 39 24; fax: +33 2 40 37 39 95.
E-mail address: Karsten.Rasim@cnrs-imn.fr (K. Rasim).
[1] Current address: The Abdus Salam International Centre for Theoretical Physics, Strada Costiera 11, 34151 Trieste, Italy.

1381-1169/$ – see front matter © 2010 Elsevier B.V. All rights reserved.
doi:10.1016/j.molcata.2010.03.021

Table 1
Ammonia adsorption energies on Pt(1 1 1), Pt(1 0 0) and Pt/Au(1 1 1) at different coverages together with literature data in brackets (in eV).

	Pt(1 1 1)	Pt(1 0 0)	Pt/Au(1 1 1)
$E_{ads}(\theta = 1/9)$	−0.92 (−0.97 [16])	−1.04 (−1.10 [16])	−0.99
$E_{ads}(\theta = 1/4)$	−0.78 (−0.71 [17], −0.75 [16])	−0.90 (−0.89 [16])	−0.81
$E_{ads}(\theta = 1/2)$	−0.55 [a]	−0.53 (−0.57 [16])	−0.58 [a]
E_{diff}	0.64	0.61	0.61

[a] marks average values of different adsorption states (see text). In the last line, the activation energy for ammonia surface diffusion is given.

reported. The system of rate equations of our microkinetic model of ammonia decomposition is presented in Section 3. The calculated stationary coverages of species participating in the decomposition reaction as well as the ammonia decomposition rate are considered as function of temperature and ammonia partial pressure. Finally, the main conclusions of our analysis are summarized in Section 4.

2. Ab initio calculations

2.1. Computational details

Reaction and activation energies, which are needed for modeling the ammonia decomposition kinetics on the catalyst surface, have been calculated within spin-polarized density-functional theory (DFT), using the Vienna ab initio simulation package (VASP) [21]. The wave functions were described by the projector-augmented wave method (PAW) [22] in the implementation of Kresse and Joubert [23]. Exchange and correlation were treated within the generalized gradient approximation (GGA) in the formulation of Perdew and Wang known as PW91 [24]. An energy cutoff of 400 eV has been used for total-energy calculations together with a mesh of $(9 \times 9 \times 1)$ k-points for integration in the first Brillouin zone. With this setup, a lattice constant of 3.98 Å has been calculated for bulk Pt (experimental: 3.92 Å [25,26]). For the bulk modulus, a value of 243 GPa has been obtained, in comparison with the value of 233 GPa found in other DFT–GGA calculations [27], and with the experimental value of 278 GPa [28]. The lattice constant for gold resulted as 4.18 Å (experimental: 4.08 Å [29]; other DFT–GGA result: 4.17 Å [30]). The catalyst surface has been modeled by a five-layer slab with a (2×2) surface cell. All atoms of the slab were allowed to relax. The vacuum gap between periodically repeated slabs was 10 Å in case of the (1 0 0) surface and 11.5 Å for the (1 1 1) surface.

The adsorption energies of ammonia and nitrogen are defined by

$$E_a(NH_3) = E_{NH_3@slab} - E_{slab} - E_{NH_3.gas}, \quad (1)$$

$$E_a(N) = \frac{E_{N@slab} - E_{slab} - E_{N_2.gas}}{2}, \quad (2)$$

where $E_{NH_3@slab}$ is the total energy of the slab with adsorbed ammonia, E_{slab} the energy of the bare slab, and $E_{NH_3.gas}$ the energy of a free ammonia molecule. The meaning of the energy terms in Eq. (2) is similar. The adsorption energies of the species NH_2 and NH are defined analogous to that of NH_3, and that of hydrogen analogous to nitrogen. For the calculations, the adsorbates were situated on only one side of the slab. It was checked that the calculated adsorption energies for the cases with ammonia adsorbed on both sides of the slab and only on one side differ less than 10 meV. Activation energies for surface diffusion of ammonia, nitrogen, and hydrogen, as well as for the dehydrogenation reactions, were calculated by the nudged elastic band (NEB) method [31,32]. The NEB-path consisted of 10–12 images in addition to the initial and final states. To reduce computation time for the NEB calculations, a $(7 \times 7 \times 1)$ k-point grid and an energy cutoff of 270 eV has been used for determining the atomic positions.

2.2. Chemisorption and surface diffusion

Ammonia decomposition is known to take place through sequential abstraction of hydrogen atoms [7,18]. Therefore, in a first step, the chemisorption of the correspondent species NH_3, NH_2, NH, as well as N and H on the catalyst surface has been investigated. Our calculated adsorption energies on the most favorable adsorption sites are listed in Tables 1 and 2 together with theoretical data from the literature for the Pt(1 1 1) and Pt(1 0 0) surfaces. There is a satisfactory agreement with the literature data. In addition, the activation energy for ammonia surface diffusion is given in Table 1. Adsorption energies of different species on less favorable adsorption sites are presented in Appendix B Supporting Information. In the following, the special configurations of the five species on the catalyst surface are described in more detail. NH_3: At low coverage, ammonia adsorption on top of Pt atoms is energetically favored on all three surfaces considered. The coverage is referred to the Pt atoms, i.e. a coverage of 1 ML corresponds to one ammonia molecule per Pt surface atom. At a coverage of 1/4 ML, on the Pt(1 1 1) and Pt/Au(1 1 1) surfaces, further ammonia molecules are adsorbed in a configuration where a second ammonia molecule (β-ammonia) is not directly bound to the surface, but to an already adsorbed molecule (α-ammonia) by a hydrogen bond [17,33–35]. Accordingly, the adsorption energies in Table 1 at 0.5 ML coverage represent an average over these two states. The calculated activation energies for ammonia diffusion on all surfaces are 0.3–0.4 eV smaller than the adsorption energies at low coverage. NH_2: The position of NH_2 on bridge sites (cf. Figs. 1–3) is energetically favored on all surfaces considered, in agreement with experimental observations [36]. Unlike the adsorption of ammonia, the adsorption energies of NH_2 on the (1 1 1) and (1 0 0) surfaces differ considerably. As for ammonia, the gold substrate does not alter the adsorption energy appreciably. The activation energy for diffusion of NH_2 between bridge sites is smaller than 0.1 eV.

NH: While Pt/Au(1 1 1) behaves similar to Pt(1 1 1) with regard to adsorption and diffusion of NH_3 and NH_2, the adsorption of NH on Pt/Au(1 1 1) is about 0.5 eV stronger than on Pt(1 1 1). This is presumably related to the preferred position of NH on hollow sites, which makes the NH binding energy sensitive to changes of the lateral lattice constant of platinum, as discussed below for nitrogen adsorption.

Table 2
Adsorption energies of different species on the most favorable sites at 1/4 ML coverage together with literature data in brackets (in eV).

E_{ads} (eV)	Pt(1 1 1)	Pt(1 0 0)	Pt/Au(1 1 1)
NH_2	−2.45 (−2.38 [18], −2.47 [16])	−3.10 (−3.14 [16])	−2.54
NH	−4.10 (−4.01 [17], −4.24 [16])	−3.97 (−4.01 [16])	4.59
N	+0.36	+0.40	−0.04
H	−0.47	−0.62	−0.81

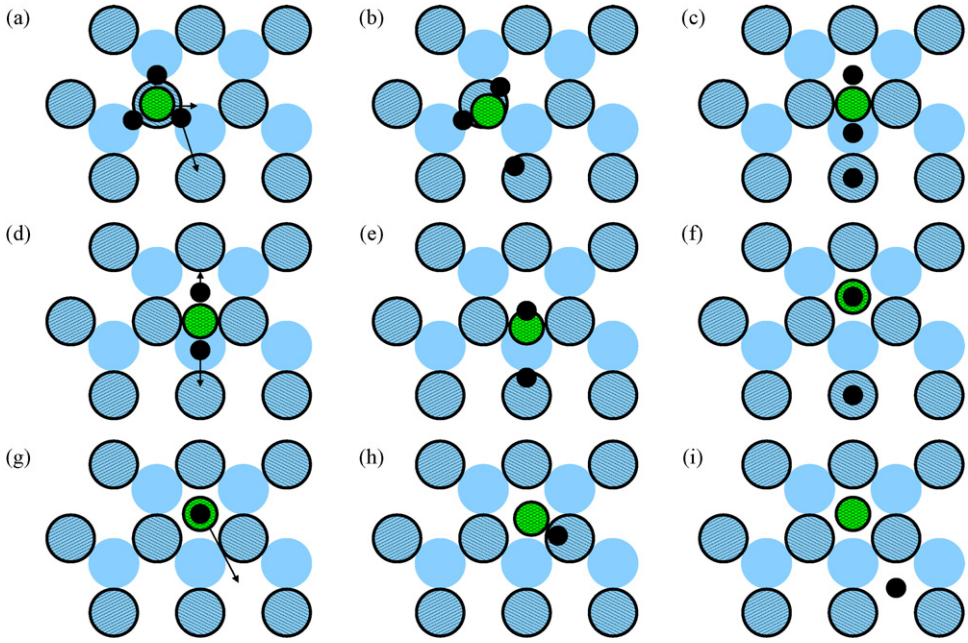

Fig. 1. Scheme of surface reactions on Pt(1 1 1). Shaded spheres, Pt atoms in the uppermost layer; full spheres, Pt atoms in the second layer; N, green; H, black. For each dehydrogenation reaction, the initial state, the transition state and the final state are shown. (a–c) $NH_3 \rightarrow NH_2 + H$; (d–f) $NH_2 \rightarrow NH + H$; (g–i) $NH \rightarrow N + H$.

Nitrogen: On Pt(1 0 0), nitrogen adsorbs preferentially in an *asymmetric* hollow configuration with substantial lattice deformation, as depicted in Fig. 4. The surface unit cell forms a kite with side-lengths of 3.14 and 2.81 Å. At a nitrogen coverage of 1/4, the distorted configuration is more stable by 0.25 eV compared to the undistorted symmetric hollow site, as already noticed by Offermans et al. [18]. At lower coverage of 1/9, the energy gain due to surface cell distortion is only 0.07 eV. The corresponding side-lengths of the surface unit cell are 2.91 and 2.78 Å. As in the case of NH, the gold substrate has a strong effect on the nitrogen adsorption energy. On Pt/Au(1 1 1), it is 0.4 eV stronger than on Pt(1 1 1). Gross and co-workers [10,11] ascribe the effect of the substrate on the adsorp-

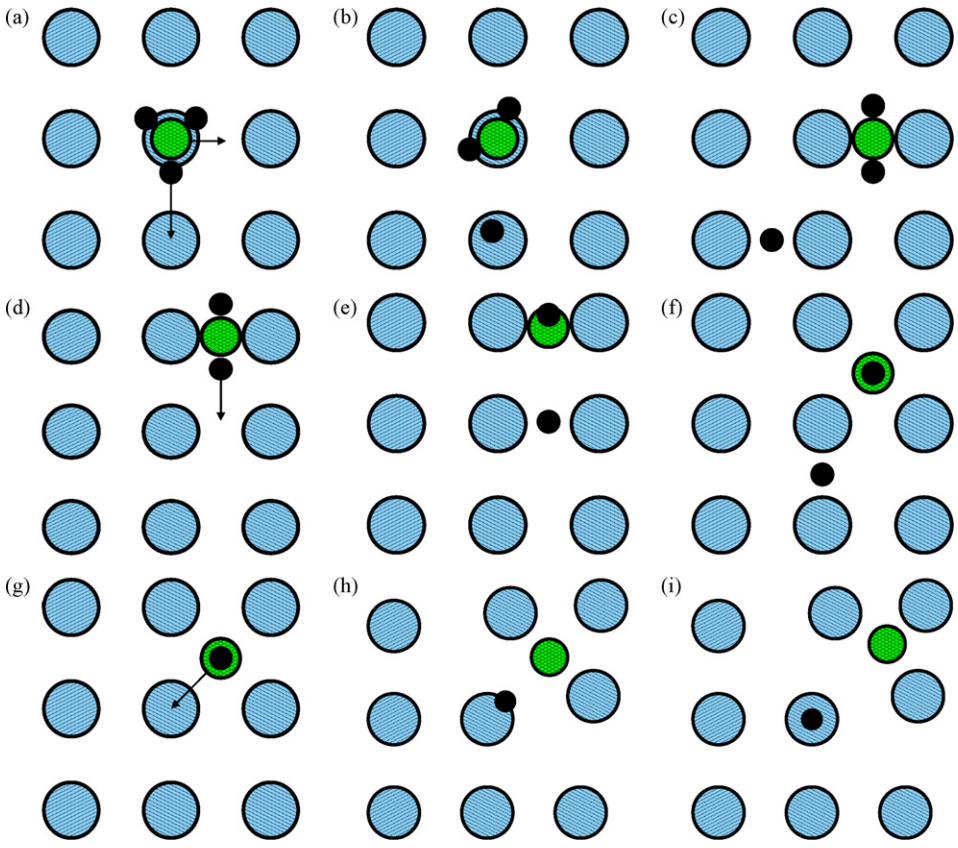

Fig. 2. Scheme of surface reactions on Pt(1 0 0) analogous to Fig. 1. Shaded spheres, Pt atoms in the uppermost layer; N, green; H, black.

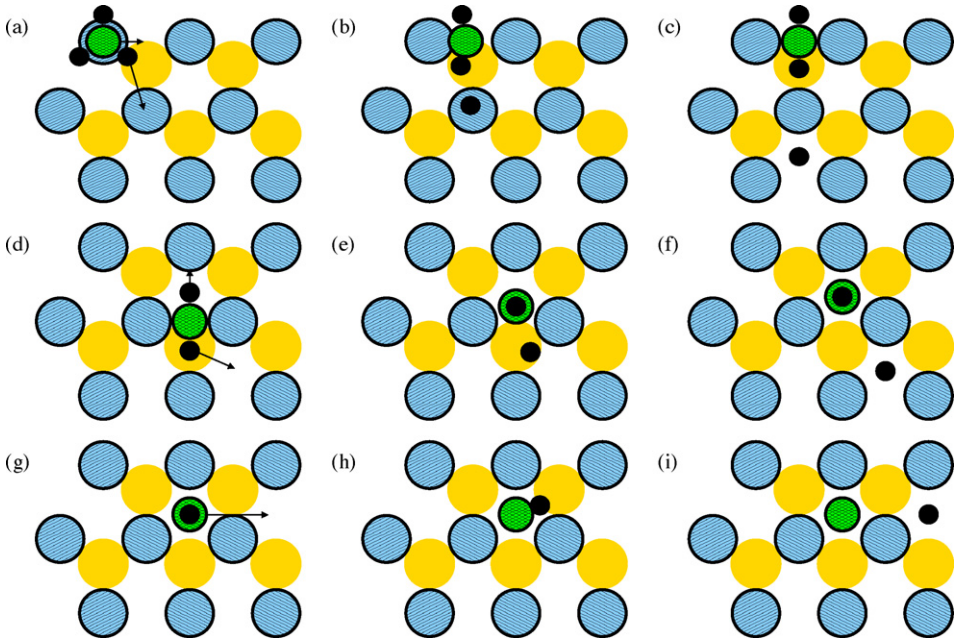

Fig. 3. Scheme of surface reactions on Pt/Au(1 1 1) analogous to Fig. 1. Shaded spheres, Pt atoms in the uppermost layer; full golden spheres, Au atoms in the second layer; N, green; H, black.

tion energy to a combination of chemical interaction and strain effect. To discriminate between these two effects, we have considered nitrogen adsorbed on the (1 1 1) surface of strained platinum with the lattice constant of Au (4.18 Å). On this artificial surface, the adsorption energy amounts to −0.13 eV, compared with −0.04 eV on Pt/Au(1 1 1) and +0.36 eV on real Pt(1 1 1). Thus, the difference in the adsorption energy between Pt/Au(1 1 1) and Pt(1 1 1) is mainly caused by the 5% expansion of the Pt-monolayer to match the lattice of the gold substrate.

Hydrogen: On Pt(1 1 1), hydrogen adsorbs on fcc-hollow and top sites with an adsorption energy of −0.47 eV, and on hcp-hollow sites with −0.43 eV. The small differences between the hydrogen adsorption energies on top and hollow sites together with the small diffusion activation energy indicate a very flat potential energy surface of hydrogen on Pt(1 1 1). On Pt(1 0 0) it adsorbs preferentially in bridge position, whereas on Pt/Au(1 1 1) the fcc-hollow site (−0.81 eV) is slightly favored over the hcp-hollow site(−0.78 eV). Also for hydrogen, the presence of the gold substrate remarkably increases the binding of hydrogen by 0.3 eV compared to Pt(1 1 1). But unlike the case of nitrogen, hydrogen binding on a strained Pt(1 1 1) surface with the lattice constant of gold is only slightly stronger than on real Pt(1 1 1), indicating a comparatively strong chemical interaction with the gold substrate (adsorption energies on artificially strained Pt(1 1 1) −0.53 eV, on real Pt(1 1 1) −0.47 eV, and on Pt/Au(1 1 1) −0.81 eV). The activation energies for hydrogen surface diffusion have been found to be about 0.1 eV on Pt(1 1 1) and Pt/Au(1 1 1), and 0.2 eV on Pt(1 0 0), in agreement with Ref. [37].

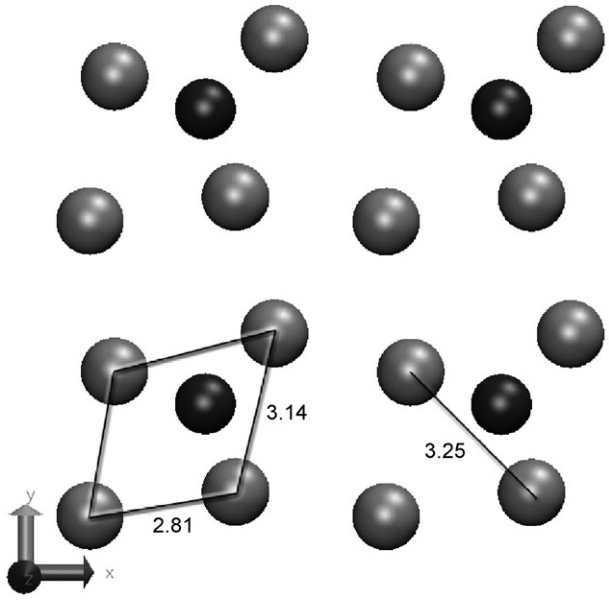

Fig. 4. Distortion of the surface unit cell on Pt(1 0 0) due to nitrogen adsorption on a hollow site at nitrogen coverage of 1/4 (black, nitrogen atoms; grey, Pt atoms in the topmost layer).

2.3. Surface reactions

Decomposition of ammonia is known to proceed by stepwise abstraction of hydrogen atoms [7]. The corresponding reactions up to complete decomposition read (*g*, in gas; *a*, adsorbed on surface):

$$NH_3(g) \rightleftharpoons NH_3(a) \quad (k_1 \text{ and } k_2) \tag{3}$$

$$NH_3(a) \rightleftharpoons NH_2(a) + H(a) \quad (k_3 \text{ and } k_4) \tag{4}$$

$$NH_2(a) \rightleftharpoons NH(a) + H(a) \quad (k_5 \text{ and } k_6) \tag{5}$$

$$NH(a) \rightleftharpoons N(a) + H(a) \quad (k_7 \text{ and } k_8) \tag{6}$$

$$2N(a) \rightleftharpoons N_2(g) \quad (k_9 \text{ and } k_{10}) \tag{7}$$

$$2H(a) \rightleftharpoons H_2(g) \quad (k_{11} \text{ and } k_{12}) \tag{8}$$

where the k_i ($i = 1$–12) denote rate constants for the forward (odd i) and backward (even i) reactions. Desorption of NH_2 and NH has been neglected in view of the high adsorption energy of these species (cf. Table 2) and the relatively low temperatures considered in the following.

To calculate the activation energies for the reactions (3)–(7), we have assumed initial, transition and final states of the corresponding reactions as shown in Figs. 1–3. The activation energies for the shown transitions have been calculated by means of the nudged

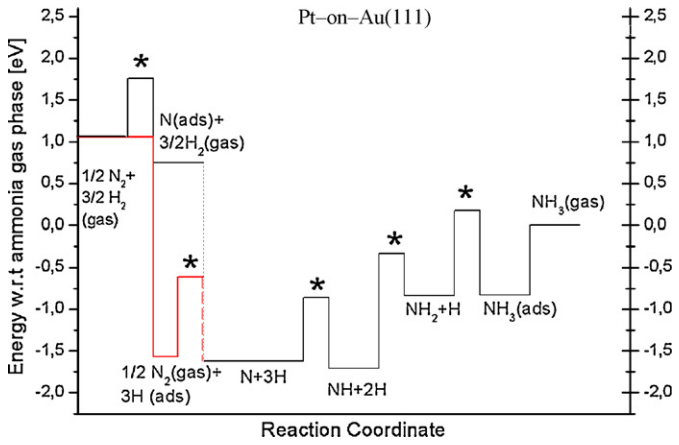

Fig. 5. Reaction energy diagram of the dehydrogenation reactions of ammonia on Pt/Au(1 1 1). The energy is referred to ammonia in the gas phase.

elastic band (NEB) method. An overview of the calculated energy landscape for the complete reaction is presented in Fig. 5 for the case of Pt/Au(1 1 1). The corresponding energy values are listed in Table 3 together with the energy values for the other two surfaces. $E_{act-direct}$ denotes the activation energy for the dehydrogenation reaction, E_{react} is the reaction energy ($E_{react} < 0$ for an exothermic reaction). The activation energy for the reverse reaction is given by $E_{act-reverse} = E_{act-direct} - E_{react}$. Similar calculations of activation energies have been reported in Refs. [16–20] for the Pt(1 1 1) and Pt(1 0 0) surfaces (cf. Table 3). Our calculated activation energies are generally slightly higher than those in Refs. [16–19], presumably due to the neglect of the zero-point energy in our calculations. Furthermore, in difference to [17], in Fig. 1c we show hydrogen on a top site as final position since the total energy has been found to be slightly lower by about 0.05 eV than in a hollow site. In this respect, we also note that the potential energy surface of hydrogen on Pt(1 1 1) is very flat as mentioned above. In the following, characteristic features of the particular reactions are summarized. $NH_3 \rightleftharpoons NH_2 + H$: The activation energies for this reaction are similar on the three surfaces with the lowest value on Pt/Au(1 1 1). $NH_2 \rightleftharpoons NH + H$: Also this reaction has the lowest activation energy on Pt/Au(1 1 1), the value of which is only half that on Pt(1 1 1). The reaction is strongly exothermic with a reaction energy of −0.87 eV. $NH \rightleftharpoons N + H$: This reaction has been found to be endothermic on all three surfaces. Both reaction and activation energies are lowest on Pt/Au(1 1 1). On the two (1 1 1) surfaces NH is energetically more stable than NH_2, whereas on Pt(1 0 0) NH_2 is more stable. $2N \rightleftharpoons N_2$: The associative desorption of nitrogen as N_2 into the gas phase is a thermally activated reaction. Since activation energies between 0.66 and 0.85 eV have been calculated for the surface diffusion of nitrogen, the associative desorption of N_2 is probably diffusion-limited, as the activation energies for association of two neighbored nitrogen atoms are lower than these values. This fact is taken into account in establishing the microkinetic model of ammonia decomposition in the next section. $2H \rightleftharpoons H_2$. Dissociative adsorption of a hydrogen molecule at a platinum surface is a spontaneous process, occurring without thermal activation. Hence, the activation energy for the associative desorption of hydrogen has been taken equal to half the adsorption energy with respect to the molecule, which lies in the range from 0.4 to 0.8 eV (cf. Table 2).

Table 3
Activation and reaction energies for the dehydrogenation reactions and for nitrogen desorption (in eV).

	$E_{act-direct}$	E_{react}
$NH_3 \rightleftharpoons NH_2 + H$		
Pt(1 0 0)	1.15 (1.05 [16], 0.93 [20])	−0.21
Pt(1 1 1)	1.09 (1.02 [16], 0.96 [17])	0.48
Pt/Au(1 1 1)	1.00	0.0
$NH_2 \rightleftharpoons NH + H$		
Pt(1 0 0)	1.02 (1.63 [16], 1.11 [20])	0.54
Pt(1 1 1)	1.26 (1.10 [16], 1.14 [17])	−0.07
Pt/Au(1 1 1)	0.50	−0.87
$NH \rightleftharpoons N + H$		
Pt(1 0 0)	0.97 (0.88 [16], 0.66 [20])	0.39
Pt(1 1 1)	1.33 (0.97 [16], 1.22 [17])	0.40
Pt/Au(1 1 1)	0.85	0.09
$N + N \rightleftharpoons N_2$		
Pt(1 0 0)	0.72	−0.64
Pt(1 1 1)	1.08	−0.36
Pt/Au(1 1 1)	1.01	0.05

In addition to the above dehydrogenation reaction via sequential H-abstraction, we have tried to find an alternative reaction path by performing an NEB run with an ammonia molecule as starting configuration and NH + 2H as final state. The minimum energy path for this run was found to consist of sequential abstraction of the two hydrogen atoms, thus confirming the sequential mechanism.

Our DFT analysis reveals that the most stable surface species are NH_3 on Pt(1 1 1), NH_2 on Pt(1 0 0) and NH on Pt/Au(1 1 1). In general, for the reaction of ammonia decomposition different metals have different rate-determining steps [7]. Our results show that, even for these rather similar systems, the highest activation energies are associated with different reaction steps: $NH \rightleftharpoons N + H$ for Pt(1 1 1) (1.33 eV), $NH_3 \rightleftharpoons NH_2 + H$ for Pt(1 0 0) (1.15 eV) and for Pt/Au(1 1 1) (1.0 eV). Since it is impossible to predict these findings a-priori, it is necessary to model the overall process to be able to assess the conversion rate and the nature of the rate-determining steps. The complicated interaction of ammonia with active metals is characterized by the fact that the most active catalysts for ammonia synthesis are not good catalysts for ammonia decomposition and vice versa [38].

3. Microkinetic model of ammonia decomposition

3.1. Kinetic equations

In the following, we propose a microkinetic model to describe the decomposition of ammonia on a catalyst surface under conditions present in a flow reactor or a gas sensing device. The ambient atmosphere consists of nitrogen (partial pressure 80 kPa) and ammonia with low concentration (typically < 1000 ppm). According to the Langmuir–Hinshelwood mechanism, the processes taking place on the catalyst surface are adsorption and desorption of ammonia, adsorption of nitrogen, the dehydrogenation reactions described above, and the associative desorption of nitrogen and hydrogen [17]. Hydrogen adsorption will be neglected, assuming that hydrogen desorption by ammonia decomposition is small compared to hydrogen evacuation in a flow reactor. Also diffusion of hydrogen into the bulk of the catalyst has not been included explicitly in our analysis. It is assumed that the spatial extension of the catalyst is in the nanometer region (nanoclusters or ultrathin films) and, therefore, an equilibrium between the hydrogen solved in the bulk and adsorbed on the surface is rapidly established. As already stated above, desorption of NH_2 and NH has been neglected because of the high adsorption energy of these species.

The temporal evolution of the coverages of all adsorbed species is described by occupation probabilities θ_A(A = NH_3, NH_2,NH,N,H) which denote the fraction of occupied adsorption sites on the catalyst surface. The considered adsorption sites on Pt(1 1 1) are on top of a metal atom for NH_3, on a bridge site for NH_2, and on a fcc-hollow site for NH and N. Concerning hydrogen, we have considered in our analysis on-top sites, as well as fcc-hollow and hcp-hollow

sites because of the negligible differences in the adsorption energy of hydrogen on these sites. On Pt/Au(1 1 1), hydrogen adsorption on-top of metal atoms is energetically less favorable and is therefore not included in the analysis. In the case of Pt(1 0 0), we have considered NH_3 on top sites, NH_2 and H on bridge sites, as well as NH and N on hollow sites. It is assumed that the adsorbates are equally distributed on the surface since surface diffusion should be fast compared to the other reactions due to smaller activation energies. The evolution equations of the coverages of all species are given here for the example of the Pt(1 1 1) surface:

$$\dot{\theta}_{NH_3} = k_1\bar{\theta}_t - k_2\theta_{NH_3} - k_3\theta_{NH_3}\bar{\theta}_b\bar{\theta}_{hf} + 3k_4\theta_{NH_2}\theta_H\bar{\theta}_t, \quad (9)$$

$$\dot{\theta}_{NH_2} = \frac{1}{3}k_3\theta_{NH_3}\bar{\theta}_b\bar{\theta}_{hf} - k_4\theta_{NH_2}\theta_H\bar{\theta}_t - k_5\theta_{NH_2}\bar{\theta}_{hf}\bar{\theta}_t + \frac{1}{3}k_6\theta_{NH}\theta_H\bar{\theta}_b, \quad (10)$$

$$\dot{\theta}_{NH} = 3k_5\theta_{NH_2}\bar{\theta}_{hf}\bar{\theta}_t - k_6\theta_{NH}\theta_H\bar{\theta}_b - k_7\theta_{NH}\bar{\theta}_{hh} + k_8\theta_N\theta_H, \quad (11)$$

$$\dot{\theta}_N = k_7\theta_{NH}\bar{\theta}_{hh} - k_8\theta_N\theta_H - k_9\theta_N\theta_N\bar{\theta}_t + k_{10}\bar{\theta}_{hf}^2, \quad (12)$$

$$\dot{\theta}_H = \frac{1}{3}k_3\theta_{NH_3}\bar{\theta}_b\bar{\theta}_{hf} - k_4\theta_{NH_2}\theta_H\bar{\theta}_t + k_5\theta_{NH_2}\bar{\theta}_{hf}\bar{\theta}_t - \frac{1}{3}k_6\theta_{NH}\theta_H\bar{\theta}_b + \frac{1}{3}k_7\theta_{NH}\bar{\theta}_{hh} - \frac{1}{3}k_8\theta_N\theta_H - \frac{1}{3}k_{11}\theta_H^2 \quad (13)$$

with the following notation for the unoccupied fraction of adsorption sites (the indices mean: *t*, top; *b*, bridge; *hf*, fcc-hollow, *hh* hcp-hollow site):

$$\bar{\theta}_t = 1 - \theta_{NH_3} - \theta_H, \quad (14)$$

$$\bar{\theta}_b = 1 - \theta_{NH_2}, \quad (15)$$

$$\bar{\theta}_{hf} = 1 - \theta_{NH} - \theta_N - \theta_H, \quad (16)$$

$$\bar{\theta}_{hh} = 1 - \theta_H. \quad (17)$$

The prefactors 3 and 1/3 in the above rate equations arise because there are three bridge sites per Pt atom for NH_2, and similarly three sites for hydrogen (top, fcc- and hcp-hollow). Analogous equations for the Pt/Au(1 1 1) and Pt(1 0 0) surfaces are given in Appendix B Supporting Information. The rate Eqs. (9)–(13) present a simplified description of ammonia decomposition, neglecting certain interactions between co-adsorbed species. For example, the sticking and adsorption of ammonia on a free top site should be affected to some extent by the presence of adsorbed NH_2 species on bridge sites neighbored to the free top site. Neglect of such effects is thought to be a reasonable approximation, especially for small coverages at higher temperatures.

The rate constants k_1 and k_{10} in Eqs. (9) and (12) describe the adsorption of ammonia and nitrogen from the gas phase. Hydrogen adsorption has been neglected (k_{12} =0) in Eq. (13) as explained above. The adsorption rate of ammonia is given by

$$k_1 = \frac{p_{NH_3}S_{NH_3}(T, \theta_{NH_3})}{n_0\sqrt{2\pi m k_B T}} \quad (18)$$

where p_{NH_3} is the ammonia partial pressure, $S(T, \theta_{NH_3})$ is the sticking coefficient of ammonia, n_0 is the area-density of top sites on the surface, and m is the mass of an ammonia molecule. The ammonia sticking coefficient has been roughly approximated by a constant value ($S_{NH_3} = 0.73$ [39]). A formula analogous to (18) holds for the rate constant k_{10} which is obtained as twice the impingement rate of N_2 molecules multiplied by the sticking coefficient which has been modeled by the expression:

$$S_{N_2} = S_0 \exp\left(\frac{-E_{act}}{k_B T}\right) \quad (19)$$

with S_0 as preexponential factor and E_{act} as activation energy for the dissociative adsorption of nitrogen [40]. According to the transition state theory (TST) [41,42], the other rate constants k_i in Eqs. (9)–(13) are given by

$$k_i = \nu_i \exp\left(\frac{-E_i}{k_B T}\right) \quad (20)$$

with the preexponential frequencies ν_i and activation energies E_i. Preexponential frequencies for the dehydrogenation reactions (4)–(6) have been determined in Ref. [19] for the Pt(1 1 1) and Pt(1 0 0) surfaces. We have used those values for an order of magnitude estimate of the ν_i for Pt(1 1 1) and Pt(1 0 0) at 500 K. The temperature dependence $\nu_i(T)$ has been approximated by a linear function. This is a good approximation at least from 500 to 700 K, as one finds by comparing with values at 700 K calculated in [19]. Preexponential frequencies for Pt(1 0 0) have also been reported recently in Ref. [20]. The calculated turnover frequencies using these recent values differ by less than an order of magnitude from those obtained using the frequencies given in [19] (see Appendix B Supporting Information, Fig. S1). Thus, the differences in the frequency data should not influence the main conclusions of our paper. Because of the lack of data, the preexponential factors in the case of the Pt/Au(1 1 1) overlayer have been estimated by those for Pt(1 1 1). To check this approximation, we calculated the normal modes of hydrogen vibrations on a hollow site, which exhibits the largest difference in the hydrogen adsorption energy on the two surfaces or, in other words, which experiences obviously the largest Au influence (cf. Table 2). The rate constants of the reverse reactions follow by considering detailed balance:

$$\frac{k_{direct}}{k_{reverse}} = \exp\left(\frac{-E_{react}}{k_B T}\right). \quad (21)$$

The preexponential frequencies for the desorption of nitrogen and hydrogen have been approximated by the standard frequency factor $k_B T/h$. The values of the parameters ν_i and E_i used in the present calculations are given in Appendix B Supporting Information. A coverage dependence of the activation energies E_i in (20) has generally been neglected except for the case of ammonia adsorption where a linear interpolation between the calculated adsorption energies at the coverages 1/9, 1/4, and 1/2 ML has been used. For ammonia coverages $> 1/2$, the adsorption energy has been set to zero for Pt(1 1 1) and Pt/Au(1 1 1).

3.2. Steady-state surface coverages

The steady-state surface coverages of all species, which are reached after a certain transient time, have been determined at temperatures up to 1300 K for different ammonia pressures of the ambient gas. To this end, the rate equations of the previous section have been integrated until steady state was reached. Supposing an ammonia concentration in the ambient gas of 100 ppm, the transient times to reach steady-state range from 500 s for Pt(1 1 1) at 450 K down to 10^{-2} s for Pt/Au(1 1 1) at 650 K, and still shorter at higher temperatures. The coverages of species presented in Fig. 6 as a function of temperature are referred to the atomic density of Pt atoms in the surface layer. This means that, besides θ_{NH_3}, θ_{NH}, and θ_N, the quantities $3\theta_{NH_2}$ and $3\theta_H$ are plotted for Pt(1 1 1), $3\theta_{NH_2}$ and $2\theta_H$ for Pt/Au(1 1 1), and $2\theta_{NH_2}$ and $2\theta_H$ for Pt(1 0 0).

The calculated ammonia coverage strongly decreases with increasing temperature on all surfaces. As can be seen in Fig. 6, each surface exhibits another dominant amid-species, namely NH on Pt(1 1 1), NH_2 on Pt(1 0 0), and nitrogen on Pt/Au(1 1 1). In the case of the Pt(1 0 0) surface, this finding is in agreement with experiments in gaseous [36] and aqueous [43] environment. For the Pt(1 1 1) surface, NH was found to be the most stable intermediate during ammonia oxidation in aqueous solution [43], confirming

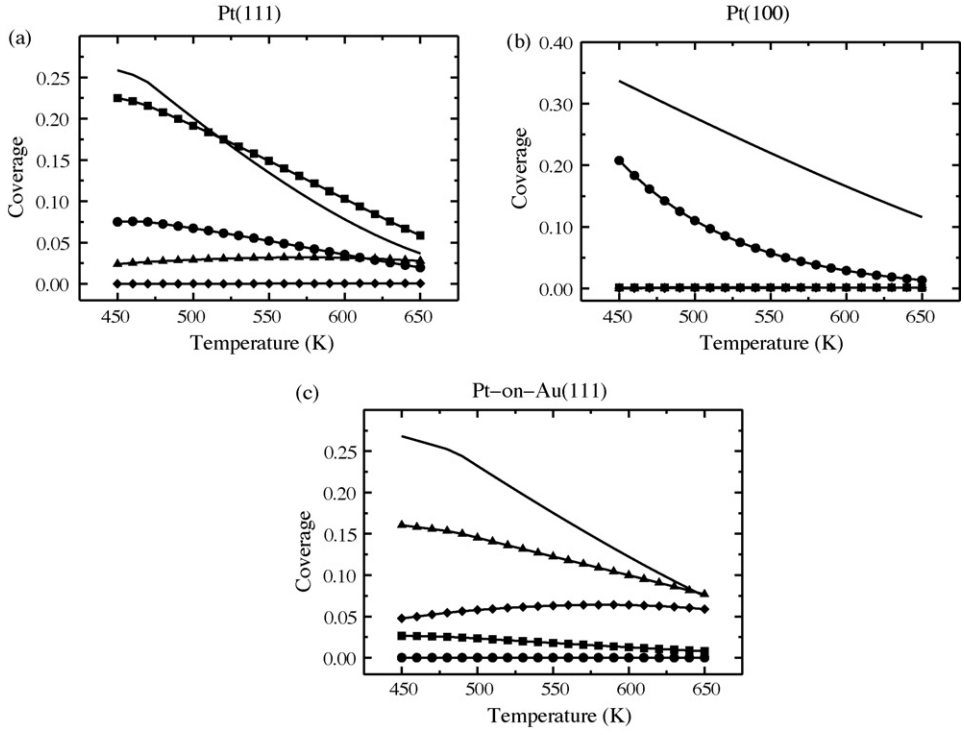

Fig. 6. Equilibrium coverages of NH_3 (solid line), NH_2 (circle), NH (square), N (triangle), and H (rhombus) on (a) Pt(1 1 1), (b) Pt(1 0 0), and (c) Pt/Au(1 1 1) as a function of temperature at 100 ppm ammonia gas concentration. On Pt(1 0 0) all curves but those of NH_3 and NH_2 lie below 0.002. Note that the coverage in this diagram is referred to the Pt surface atoms (see text for explanation).

our results. The predominance of NH on Pt(1 1 1) and of NH_2 on Pt(1 0 0) is suggested by their high adsorption energies compared to the other species (cf. Tables 1 and 2). However, on Pt/Au(1 1 1), the predominant intermediate species is obviously kinetically determined.

3.3. Ammonia decomposition rate

The ammonia decomposition rate is usually characterized by the turnover frequency (TOF) which has been derived here from the hydrogen desorption flux. For the Pt(1 1 1) surface, the turnover frequency (in molecules per unit time and unit area) results as (cf. Eq. (13)):

$$\mathrm{TOF} = \frac{1}{3} k_{11} \theta_{\mathrm{H}}^2 n_0 \tag{22}$$

where the factor 1/3 is due to the N:H ratio of NH_3.

The calculated steady-state values of the turnover frequencies on all surfaces considered are shown in Fig. 7 as Arrhenius plots. At high temperature, the turnover frequency is nearly independent of the temperature, whereas at low temperature an Arrhenius behavior is found. In the low-temperature region, an apparent activation energy:

$$E_{\mathrm{act,app}} = k_B T^2 \frac{\mathrm{d}\ \ln(\mathrm{TOF})}{\mathrm{d}T}, \tag{23}$$

has been derived from the Arrhenius plots. This activation energy characterizes the overall temperature dependence of the ammonia decomposition process. The lowest value of 0.96 eV has been obtained for Pt/Au(1 1 1), compared to 1.14 eV for Pt(1 0 0) and 1.28 eV for Pt(1 1 1). These values are remarkably similar to the highest activation energies for the surface reactions on each surface (cf. Table 3). This suggests that in the low-temperature region the apparent activation energy is determined by that of the rate-limiting step.

Measurements of turnover frequencies on polycrystalline platinum wires in a wide range of ammonia pressures have been reported in Ref. [44]. To compare our model predictions with those measurements, the turnover frequencies on Pt(1 1 1) have been calculated for the ammonia partial pressures considered in [44], ranging from 10^{-6} to 0.5 Torr. The corresponding Arrhenius plots of the turnover frequency in Fig. 8 reveal that the turnover frequency at low temperature and high ammonia pressure is nearly independent of the pressure. Our calculated turnover frequencies are one to two orders of magnitude higher than the measurements in [44], with less pronounced differences at low temperature. However, characteristic features of the experimental data are reproduced by our calculations as for example the saturation of the turnover frequency above 600 K at intermediate ammonia pressure. Also

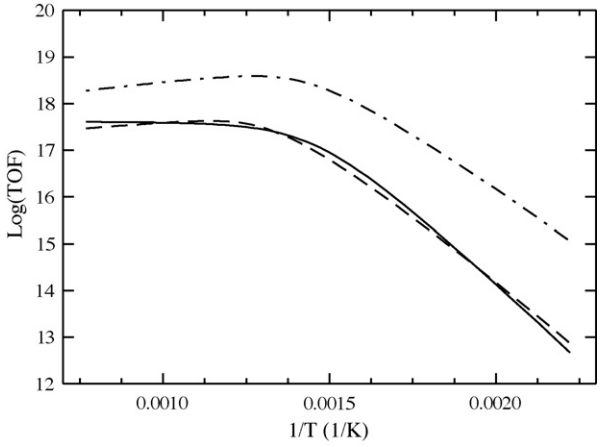

Fig. 7. Arrhenius plots of the turnover frequency (TOF) as a function of reciprocal temperature on Pt(1 1 1) (solid line), Pt(1 0 0) (dashed), and Pt/Au(1 1 1) (dot-dashed) at 100 ppm ammonia gas concentration. The TOF is given in molecules/(cm^2 s).

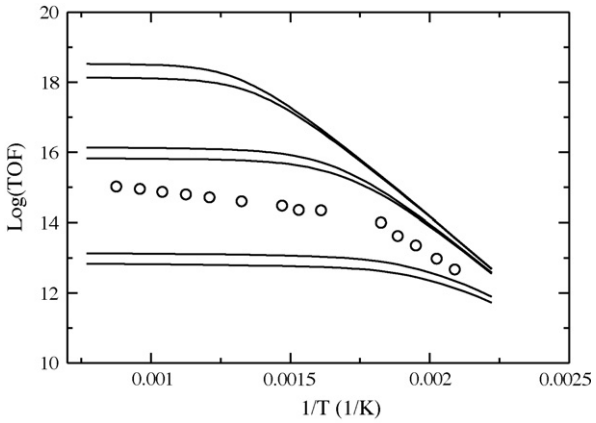

Fig. 8. Arrhenius plots of the turnover frequency (TOF) on Pt(1 1 1) as a function of reciprocal temperature for different ammonia partial pressures (calculated values, solid line; one example of the experimental values in Ref. [44], circles). From the bottom, the solid lines refer to an ammonia partial pressure of 10^{-6} Torr, 2×10^{-6}, 10^{-3}, 2×10^{-3}, 0.2, 0.5. The circles refer to an ammonia partial pressure of 10^{-3} Torr. The TOF is given in molecules/(cm^2 s).

as in the experiment, the vertical separation of the three pressure branches in Fig. 8 is roughly equal on the logarithmic scale. Actually one could expect that the theoretical turnover frequencies are smaller than the experimental values since the Pt(1 1 1) surface is probably less active than more loosely packed or stepped surfaces. On the other hand, the experimental measurements can be affected by poisoning of the catalyst surface lowering their activity.

Another possible reason for differences between our model predictions and experimental findings could be that in our calculations quantum tunneling as a mechanism for hydrogen abstraction [45] has been neglected. To estimate the corresponding correction to the reaction rates within TST, we have calculated the semi-classical Wigner correction [45,46] according to which the first-order correction to the reaction rate is a multiplicative factor $k_{\mathrm{Wigner}} = 1 + |\hbar\omega\beta|^2/24$ where ω is the imaginary frequency at the transition state and $\beta = (kT)^{-1}$. With the imaginary frequencies for hydrogen abstraction from NH_x reported in [47], the correction factor k_{Wigner} results as 3.1 at 450 K, 1.75 at 600 K, and much lower at higher temperatures. A correction factor equal to three is certainly within the uncertainty of our knowledge of the rate constants k_i.

The accuracy of our calculated steady-state coverages (Fig. 6) and turnover frequencies (Figs. 7 and 8) is limited by the inexact knowledge of the rate constants k_i in the microkinetic Eqs. (9)–(13). The rate constants (20) include frequency prefactors and activation energies. To assess how strong our calculated coverages and turnover frequencies depend on the particular choice of these two parameters, we have performed test calculations with modified parameters. As an example, the Pt(1 1 1) surface has been considered in the temperature range from 450 to 1300 K at 100 ppm ammonia gas concentration. In a first set of calculations, the prefactors ν_i of all reactions with activation energy higher than 1 eV (i.e. ν_3, ν_5, ν_6, ν_7, and ν_9) have been enlarged and diminished, respectively, by a factor of 10. This changes the turnover frequency by roughly a factor of 10. The steady-state coverages display a different behavior. The coverage of NH_3 does not change (it is obviously determined by the adsorption–desorption equilibrium of ammonia), while that of NH changes from 0.14 through 0.23 to 0.35 from low to high prefactors at 450 K. The hydrogen coverage remains below 0.01 for all parameter sets. Changes induced by a modification of only a few of these prefactors, as well as of all prefactors with reaction barriers below 1 eV, lead to smaller changes of coverages and turnover frequency. In a second set of calculations, the activation energies E_i of surface reactions have been modified. First, activation energies higher than 1 eV have been raised or lowered by 0.1 eV. At a temperature of 450 K, the turnover frequencies for raised activation energies differ from that with lowered energies by three orders of magnitude. This difference diminishes with increasing temperature. At 650 K, the turnover frequencies differ less than a factor of 10. The apparent activation energy for the low temperature branch of the turnover frequencies in Fig. 8 changes by ±0.14 eV for the two cases. In summary,

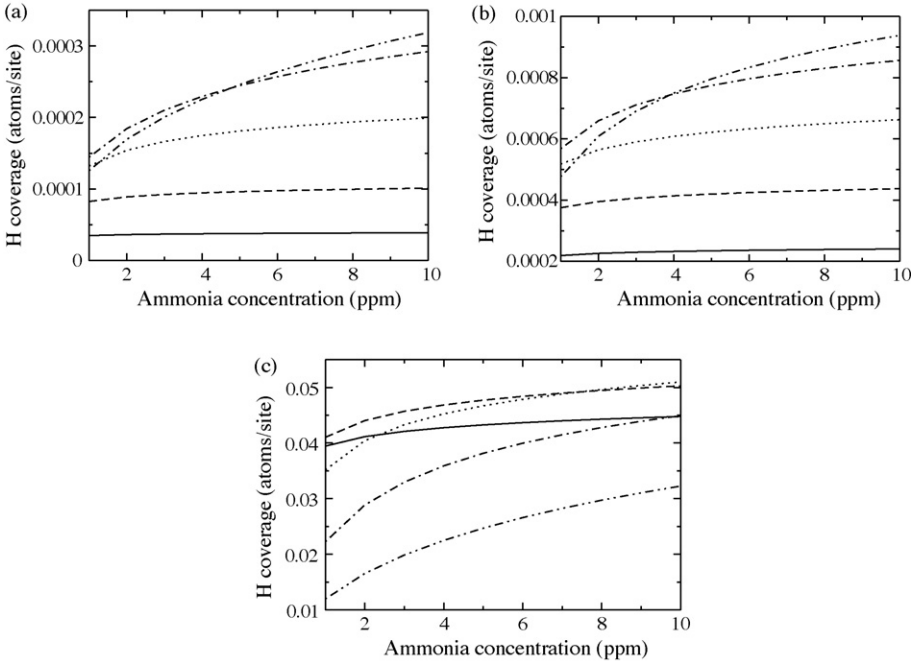

Fig. 9. Hydrogen equilibrium coverage per surface Pt atom as a function of ammonia concentration in the gas phase at different temperatures on (a) Pt(1 1 1), (b) Pt(1 0 0), and (c) Pt/Au(1 1 1). Temperatures: 450 K (solid), 500 K (dashed), 550 K (dotted), 600 K (dot-dashed), and 650 K (double dot-dashed).

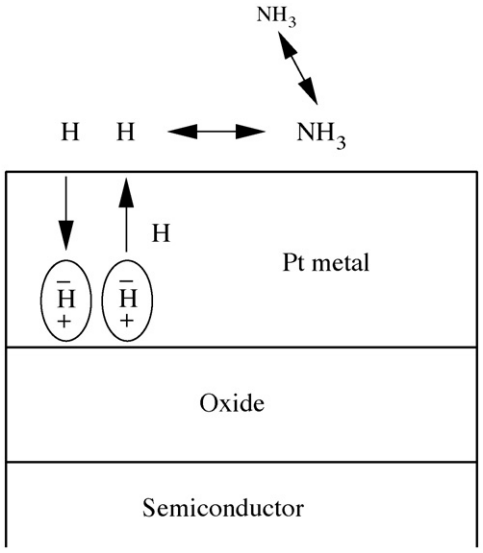

Fig. 10. Schematic view of a gas sensor. Hydrogen present on the catalyst surface partly diffuses to the interface between Pt and the underlying oxide. This creates a potential difference at the interface that can be used to estimate the hydrogen coverage and, therefore, the ammonia pressure.

the performed test calculations with modified rate constants show that the uncertainty in the knowledge of the corresponding activation energies and frequency prefactors does not dramatically influence our predictions on the ammonia decomposition kinetics.

3.4. Dependence of hydrogen coverage on ammonia gas pressure

The decomposition of ammonia on a catalyst surface can serve as mechanism of ammonia detection. A possible approach for this purpose is the measurement of the hydrogen coverage on the catalyst surface. To achieve high measuring sensitivity, the hydrogen coverage on the catalyst surface should strongly and immediately respond to changes of the ammonia concentration in the ambient gas. In the temperature range from 450 to 600 K, the steady-state hydrogen coverages on the catalyst surfaces considered differ by one order of magnitude, being largest on Pt/Au(1 1 1) and smallest on Pt(1 1 1) (cf. Fig. 9). This correlates with the hydrogen adsorption energies of −0.81 eV on Pt/Au(1 1 1), −0.62 eV on Pt(1 0 0), and −0.47 eV on Pt(1 1 1). The measuring sensitivity is the larger the steeper the slope of the curves in Fig. 9. The slope increases with increasing temperature. Again, the Pt/Au(1 1 1) surface shows the most suited curve progression. Already at 600 K the slope is much larger than for the other surfaces.

For detection of hydrogen coverage changes, the voltage shift at the catalyst surface can be measured in real sensors [48]. The voltage shift is caused by accumulation of protons at the interface between platinum and the underlying oxide, as depicted in Fig. 10. According to Salomonsson et al. [49], the voltage shift ΔV in the capacitance–voltage characteristics of a sensing device is related to changes of the hydrogen area-density Δn_i at the interface by $\Delta V = (\mu/\epsilon)\Delta n_i$, where μ is the dipole moment of an interface-adsorbed hydrogen atom and ϵ is the permittivity of the oxide. The relationship between the surface and interface area-densities depends on the special metal-oxide system (see e.g. [49]). This problem is beyond the scope of the present work. However, the hydrogen interface coverage generally increases with the surface coverage. Considering for example an ammonia concentration of 1 ppm at a temperature of 450 K (cf. Fig. 9), the surface coverage on Pt(1 0 0) is about seven times larger than on Pt(1 1 1), and 1000 times larger on Pt/Au(1 1 1). The curves in Fig. 9 reveal high slopes and correspondingly high measuring sensitivity at low ammonia concentration. On Pt(1 1 1) and Pt(1 0 0), the hydrogen coverage changes only weakly at higher ammonia concentration, especially at low temperatures. Comparing the considered catalyst surfaces at ammonia concentration from 1 to 10 ppm and at temperatures 600 and 650 K, the Pt/Au(1 1 1) surface clearly shows the highest measuring sensitivity.

4. Conclusions

Ammonia decomposition on platinum has been investigated within a microkinetic model. In particular, the Pt(1 1 1) and Pt(1 0 0) surfaces have been compared with a Pt overlayer on a Au(1 1 1) substrate. The rate constants in the microkinetic model have been estimated on the basis of ab initio calculations of the corresponding reaction and activation energies. Frequency factors in the rate constants have been adopted from calculations in [19] for Pt(1 0 0) and for Pt(1 1 1). The latter data have been applied also to Pt/Au(1 1 1).

The solution of our microkinetic model reveals high steady-state coverages of NH_2 on Pt(1 1 1) and of NH on Pt(1 0 0) in agreement with experimental observations [36,43]. Calculations of turnover frequencies on Pt(1 1 1) as a function of temperature and ammonia partial pressure reflect characteristic features as observed in experiments on polycrystalline platinum wires [44]. For example, at low temperature and high ammonia pressure, a zero-order dependence of the ammonia decomposition rate on the ammonia pressure has been found. At high temperature, the decomposition rate becomes nearly independent of the temperature on all surfaces considered. This weak temperature dependence is in agreement with the experimental results in Refs. [44,50]. A decrease of the turnover frequencies at temperatures above 750 K has been found, however, in Ref. [39].

Interesting results of our theoretical study have been obtained for the bimetallic system Pt/Au(1 1 1). Comparing the different catalyst surfaces, our calculations predict considerably higher ammonia decomposition rates on Pt/Au(1 1 1). Moreover, the model suggests that the Pt/Au(1 1 1) system displays a comparatively sensitive dependence of the hydrogen coverage on the ammonia pressure at a nitrogen pressure of 80 kPa and for ammonia concentrations of about 1–10 ppm. In view of these theoretical findings, the Pt/Au(1 1 1) system might be suitable for the design of ammonia-sensing devices or other catalytic applications, provided that the operation temperature is sufficiently low so that this metastable system is not destroyed by diffusion of platinum into the gold substrate. Exploration of its stability range needs further theoretical and experimental investigations.

Acknowledgments

Computing resources were provided by the Center for Information Services and High Performance Computing (ZIH) of the Dresden University of Technology, Germany. NS acknowledges financial support by the Austrian FWF within the joint research program “Nanoscience at Surfaces”. KR is very grateful to Arezoo Dianat for the help in using VASP.

Appendix A. Supplementary data

Supplementary data associated with this article can be found, in the online version, at doi:10.1016/j.molcata.2010.03.021.

References

[1] V. Smil, Nature 400 (1999) 415.
[2] R. Schlögl, Angew. Chem. Int. Ed. 42 (2004).

[3] J.A. Pool, E. Lobkovsky, P.J. Chirik, Nature 427 (2004) 527.
[4] C.H. Christensen, T. Johannessen, R.Z. Sorensen, J.K. Norskov, Catal. Today 111 (2006) 140.
[5] A. Wojcik, H. Middleton, I. Damopoulos, J. Van Herle, J. Power Sources 118 (2003) 342.
[6] M.V. Twigg, Appl. Catal. B: Environ. 70 (2007) 2.
[7] J.C. Ganley, F.S. Thomas, E.G. Seebauer, R.I. Masel, Catal. Lett. 96 (2004) 117.
[8] T.V. Choudhary, A.K. Santra, C. Sivadinarayana, B.K. Min, C.-W. Yi, K. Davis, D.W. Goodman, Catal. Lett. 77 (2001) 1.
[9] M.O. Pedersen, S. Helveg, A. Ruban, I. Stensgaard, E. Laegsgaard, J.K. Norskov, F. Besenbacher, Surf. Sci. 426 (1999) 395.
[10] Y. Gohda, A. Gross, J. Electroanal. Chem. 607 (2007) 47.
[11] Y. Gohda, A. Gross, Surf. Sci. 601 (2007) 3702.
[12] O.R. Inderwildi, S.J. Jenkins, D.A. King, Surf. Sci. L103 (2007).
[13] A. Michaelides, Surf. Sci. 601 (2007) 3529.
[14] S. Kumar, S. Zou, Langmuir 23 (2007) 7365.
[15] P. Liu, X. Ge, R. Wang, H. Ma, Y. Ding, Langmuir 25 (2009) 561.
[16] G. Novell-Leruth, A. Valcarcel, A. Clotet, J.M. Ricart, J. Perez-Ramirez, J. Phys. Chem. B 109 (2005) 18061.
[17] W.K. Offermans, A.P.J. Jansen, R.A. van Santen, Surf. Sci. 600 (2006) 1714.
[18] W.K. Offermans, A.P.J. Jansen, R.A. van Santen, G. Novell-Leruth, J.M. Ricart, J. Perez-Ramirez, J. Phys. Chem. C 111 (2007) 17551.
[19] G. Novell-Leruth, A. Valcarcel, J. Perez-Ramirez, J.M. Ricart, J. Phys. Chem. C 111 (2007) 860.
[20] G. Novell-Leruth, J.M. Ricart, J. Perez-Ramirez, J. Phys. Chem. C 112 (2008) 13554.
[21] G. Kresse, J. Furthmüller, Comput. Mater. Sci. 6 (1996) 15.
[22] P.E. Blöchl, Phys. Rev. B 50 (1994) 17953.
[23] G. Kresse, D. Joubert, Phys. Rev. B 59 (1999) 1758.
[24] J.P. Perdew, J.A. Chevary, S.H. Vosko, K.A. Jackson, M.R. Pederson, D.J. Singh, C. Fiolhais, Phys. Rev. B 46 (1992) 6671.
[25] H. Okamotot (Ed.), Phase Diagram of Binary Iron Alloys, ASM International, 1993.
[26] E.A. Brandes, Smithells Metal Reference Book, 6th ed., Butterworth, London, 1983.
[27] L. Colombi Ciacchi, W. Pompe, A. De Vita, J. Phys. Chem. B 107 (2003) 1755.
[28] C. Kittel, Introduction to Solid State Theory, Wiley, New York, 1986.
[29] P. Eckerlin, H. Kandler (Eds.), Landolt-Börnstein, 6th ed., Springer, Berlin, 1971, vol. III/6, p. 2.
[30] C. Bercegeay, S. Bernard, Phys. Rev. B 72 (2005) 214101.
[31] G. Mills, H. Jonsson, G.K. Schenter, Surf. Sci. 324 (1995) 305.
[32] G. Henkelman, H. Jonsson, J. Chem. Phys. 113 (2000) 9978.
[33] G.B. Fisher, Chem. Phys. Lett. 79 (1981) 3.
[34] M. Garcia-Hernandez, N. Lopez, I.D. Moreira, J.C. Paniagua, F. Illas, Surf. Sci. 430 (1999) 18.
[35] D.R. Jennison, P.A. Schultz, M.P. Sears, Surf. Sci. 368 (1996) 253.
[36] D.Yu. Zemlyanov, M.Yu. Smirnov, V.V. Gorodetskii, Surf. Sci. 391 (1997) 37.
[37] S.C. Badescu, P. Salo, T.Ala. Nissila, S.C. Ying, K. Jacobi, Y. Wang, K. Bedürftig, G. Ertl, Phys. Rev. Lett. 88 (2002) 136101.
[38] A. Boisen, S. Dahl, J.K. Norskov, C.H. Christensen, J. Catal. 230 (2005) 309.
[39] W.L. Guthrie, J.D. Sokol, G.A. Somorjay, Surf. Sci. 109 (1981) 390.
[40] I. Chorkendorff, J.W. Niemantsverdriet, Concepts of Modern Catalysis and Kinetics, Wiley-VCH, 2007, p. 272.
[41] H. Eyring, J. Chem. Phys. 3 (1935) 107.
[42] S. Gonzalez, D. Loffreda, P. Sautet, F. Illas, J. Phys. Chem. C 111 (2007) 11376.
[43] V. Rosca, M.T.M. Koper, Phys. Chem. Chem. Phys. 8 (2006) 2513.
[44] W. Tsai, J.J. Vajo, W.H. Weinberg, J. Phys. Chem. 89 (1985) 4926.
[45] A. Fernandez-Ramos, J.A. Miller, S.J. Klippenstein, D.G. Truhlar, Chem. Rev. 106 (2006) 4518.
[46] E.P. Wigner, Z. Phys. Chem. Abt. B 19 (1932) 203.
[47] A.M. Mebel, L.V. Moskaleva, M.C. Lin, J. Mol. Struct. Theochem. 461–462 (1999) 223.
[48] L.-G. Petersson, H. Dannetun, J. Fogelberg, I. Lundström, Appl. Surf. Sci. 27 (1986) 275.
[49] A. Salomonsson, M. Eriksson, H. Dannetun, J. Appl. Phys. 98 (2005) 014505.
[50] J.L. Gland, E.B. Kollin, Surf. Sci. 104 (1981) 478.